Domain evolution in epitaxial (001) Pb(Zr,Ti)O_{3} ultrathin films under an electric field applied along the [111] direction

D. Sichuga and L. Bellaiche

Domain evolution in epitaxial (001) Pb(Zr,Ti)O$_3$ ultrathin films under an electric field applied along the [111] direction

D. Sichuga[1] and L. Bellaiche[2]

[1]*Physics Department, Augusta Technical College, Augusta, Georgia 30906, USA*
[2]*Institute for Nanoscience and Engineering and Physics Department, University of Arkansas, Fayetteville, Arkansas 72701, USA*

The multidomain structure evolution in Pb(Zr,Ti)O$_3$ ultrathin films subject to an electric field applied along the pseudo-cubic [111] direction is investigated via the use of an effective Hamiltonian. Varying the magnitude of this electric field (that possesses both in-plane and out-of-plane components) leads to the formation of five different states, whose microstructures and properties are revealed here. Such variation also makes the polarization changing not only in magnitude but also in direction. The field-induced correlation between the polar distortions and the oxygen octahedral tilting is also discussed as an important factor affecting the polarization.

I.   INTRODUCTION

Ferroelectric (FE) materials retain their popularity with theoretical and experimental research as new features on a nanoscale level are continuously discovered inspiring the design and further miniaturization of electronic devices (see, e.g., Refs. 1-12 and references therein). For instance, a remarkable property of epitaxial FE ultrathin films, the formation of 180° stripe domains,[13-15] has recently received a new development in the study of Pb(Zr$_{1-x}$Ti$_x$)O$_3$ (PZT) solid solution – one of the most promising ferroelectrics.[16-18] In such a system, varying misfit strain causes vital transformations of laminar nanodomains leading to novel structural phases.[19,20] Additionally, the oxygen octahedral tilting, which is also termed the *antiferrodistortive* (AFD) motion,[21-27] is able to significantly affect the configuration of dipolar nanostripes.[19] It happens because of the competing nature[28] of the coupling between FE and AFD degrees of freedom, with the magnitude of latter being dependent on the Zr content in the alloy.[19] Therefore, the aforementioned factors – the misfit strain and Zr content – may be employed to alter the properties of a multidomain structure. Understandably, these factors are inherent properties of an epitaxial film and cannot be changed once the fabrication of the film is complete. For that reason, continuous adjustments of nanodevice features should be based on external factors that are able to modify the dipoles' configuration in domains to strengthen their particular properties on demand. Such an influence on a ferroelectric film, as a part of an electronic device, can be delivered by a homogenous electric field. Indeed, an electric field integrated into

1

domain environment, strong enough to distort the depolarizing field responsible for the stripe domains presence, will change the overall picture of a multidomain setting, eventually transforming it into a single *monodomain* arrangement. Clearly, the impact on the film features will depend on the magnitude but also *direction* of the external field. For instance, it was shown that such a field progressing along the *out-of-plane* [001] direction overpowers the misfit-strain-induced depolarizing field and eventually completely rearranges the dipoles configuration into a monodomain (via the formation of electric *bubbles*) when reaching a certain critical value.[29]

Surprisingly, to the best of our knowledge, nothing is known about the application of an electric field deviating from the out-of-plane direction on the properties of FE thin films possessing nanostripe domains. This contrasts with the case of magnetic films for which the application of a magnetic field having both in-plane and out-of-plane components has been demonstrated to induce novel features.[30,31]

The aim of this study is twofold: (1) to reveal the influence of an external field applied along the high-symmetry [111] direction on a (001) PZT film's morphology; (2) to investigate the possibility of managing the macroscopic properties (such as polarization) of this system using an external electric field. As a consequence of structural alterations, we were able to observe the system's transition through several different states with specific and peculiar dipoles' arrangements – the *configuration phases*. During this evolution, change in the dipoles' alignment leads to transformation of the net polarization from a zero value initially to a strong nonzero assertion in the final state, presenting the vulnerability of polarization to an external field influence. The development and mutual correlation of both polar and non-polar (AFD motion) degrees of freedom are also analyzed in this report as a significant factor able to affect the polarization.

The manuscript is organized in the following way. In Section II, we discussed the effective Hamiltonian used in Monte Carlo simulations for this study. The analysis of obtained results leading to various predictions is presented in Section III. At this point, we revealed the evolution of the system through different states supplemented by the changes in polarization, and also exposed how the external field affects the relationship between the system's FE and AFD degrees of freedom. The results of the present investigation are summarized in Section IV.

II.   METHOD

We model, at T = 10 K, epitaxial (001) 4.8-nm-thick films made of disordered PZT solid solutions possessing a Ti content of 48%. Such composition corresponds to the middle of the morphotropic phase boundary in PZT bulk.[16,17,21] We use a 12×12×12 supercell that is periodic along the *x* and *y* axis (that coincide with the [100] and [010] pseudocubic directions, respectively) and that is finite along the nonperiodic *z* axis (which lies along the [001] pseudocubic direction), in order to address surface effects existing in a real film. This system is mimicked to be under open-circuit (OC) electrical boundary conditions and under an applied misfit compressive strain of –2%. When placed under such conditions, ferroelectric films are known to have stripe domains.[13,14] The E_{tot} total energy of the studied system is provided by the first-

principles-derived effective Hamiltonian, E_{Heff}, of Ref. 32 with the exceptions of using OC (rather than short-circuit) electrical boundary conditions[33] and applying an electric field, $\boldsymbol{E}$, being oriented along [111] and ranging in magnitude from 10^5 V/m to 10^{10} V/m. Practically, such energy is given by:

$$E_{tot}\left(\{\boldsymbol{u}_i\},\{\boldsymbol{v}_i\},\{\eta_H\},\{\boldsymbol{\omega}_i\},\{\sigma_j\}\right) = E_{Heff}\left(\{\boldsymbol{u}_i\},\{\boldsymbol{v}_i\},\{\eta_H\},\{\boldsymbol{\omega}_i\},\{\sigma_j\}\right)$$
$$+\ \frac{1}{2}\ \beta\ \sum_i\langle\boldsymbol{E}_{dep}\rangle\ \cdot\ Z^*\boldsymbol{u}_i - \sum_i\boldsymbol{E}\cdot Z^*\boldsymbol{u}_i, \quad (1)$$

where the variable $\boldsymbol{u}_i$ is the local soft-mode for each unit cell i, and produces an electric dipole $Z^*\boldsymbol{u}_i$ localized on the Ti (or Zr) site in the unit cell i after being multiplied by the Z^* Born effective charge associated with the local soft-mode.[34] The $\boldsymbol{v}_i$'s are the inhomogeneous strain-related variables,[34] η_H is the homogeneous strain tensor,[34] and $\boldsymbol{\omega}_i$ is a *pseudo-vector* (also localized on Ti or Zr sites) that characterizes the direction and magnitude of AFD motion in the unit cell i. For instance, $\boldsymbol{\omega}_i = 0.1\boldsymbol{z}$ corresponds to an oxygen octahedral rotation of the cell i by 0.1 radians about the z axis with $\boldsymbol{z}$ being the unit vector along [001]. Finally, $\sigma_j = +1$ (respectively, -1) symbolizes the presence of a Zr (respectively, a Ti) atom at the site j of the supercell. The second term in the right side of Eq. (1) represents the depolarizing energy[33] and involves the screening parameter β that controls the magnitude of the residual depolarizing field; that is, $\beta = 0$ corresponds to ideal OC conditions with maximum magnitude of the $\langle\boldsymbol{E}_{dep}\rangle$ depolarizing field (employed in our investigation), and an increase in screening parameter reduces the residual depolarizing field value. Lastly, the third term in Eq. (1) imitates the effect of the external homogeneous $\boldsymbol{E}$ electric field on properties of the system.[35]

The couplings between all the listed above variables are included in the effective Hamiltonian[21] that is employed in Monte Carlo simulations with a number of sweeps being up to 10^5. More detailed information about the numerical method presently used can be found in Refs. 18,19,21,34.

III.   RESULTS AND DISCUSSION

A. Domain phase transformation

As was pointed out in the methodology section above, the investigation was performed for the system placed in the ground state, that is, at 10 K, instead of a room-temperature setting. Such "ideal conditions" let us get the most comprehensive picture of the physics of stripe domains evolution stimulated by the external field. First of all, cooling down the sample allowed avoiding the influence of thermal motion on the dipoles' behavior that can be substantial, making the stripe domains less well defined. The latter means that some details of phase transitions and the evolution of domains' morphology would be masked by the thermal deviations.

In addition, in the ground state, the system possesses both degrees of freedom – AFD motion and polar distortion. Although being an intrinsic property of such a system as PZT, the *long-range-ordered* AFD motions do not exist at room temperature and the polarization is the only order parameter. For the PZT composition

used in our investigation, the AFD condensation takes place at a temperature just below 200 K in the bulk.[21] Since the oxygen octahedral rotation is able to compete with the dipoles' behavior,[28] impact their collective arrangement and, finally, the polarization of the system, the insertion of AFD motions into the computational scheme becomes imperative.

Clearly, both of the listed above reasons made the cooling down of the film in this study crucial. The obtained low-temperature results may be used to qualitatively foresee the behavior of the system at the room temperature.

Figure 1 provides the absolute value (averaged over all the sites) of the Cartesian components of the individual dipole moments as a function of magnitude of the external electric field applied along the [111] direction. Figure 1 also reports the corresponding average value of the *magnitude* of the local dipoles. The analysis of dipoles' behavior allows an introduction of *five phases* through which the system evolves while transitioning from the initial *multidomain* state to a *monodomain* state as its final destination: (1) the *stripe domains* (SD) phase that lasts up to the field of $\sim 10^8$ *V/m* and progresses into (2) *dipolar waves* (DW) phase ending for an electric field of $\sim 5 \times 10^8$ *V/m*, (3) a *bubbles phase* (BP) that extends up to the field of *1.4×10^9 V/m* leading the system into (4) a *transitional phase* (TP), which has an upper boundary for a critical field slightly above *2×10^9 V/m,* and the (5) *monodomain* (MD) phase – the last one in evolution of the system. Note that the identification of each phase is based on the assessment of the averaged *magnitude* and *direction* of dipoles, correlated with their *collective arrangement* in the supercell – as illustrated by the diagrams and atomistic images presented in this report.

Interestingly, the formation of *bubbles* has been previously predicted also for ferroelectric thin films under an electric field applied along the "traditional" [001] direction[29] unlike the DW and TP states. These latter phases are thus specific to cases for which the applied electric field possesses both *in-plane* and *out-of-plane* components.

Let us now provide more details about the five phases and their field-induced evolution. When no external electric field is applied, the PZT ultrathin film exhibits 180 degrees, out-of-plane nanostripe domains that alternate along the *y* axis [see Fig. 2(a)]. As consistent with the nanodomains' morphology,[13,14] the largest dipole's component is along the *z* axis, and the averaged values of the magnitude of the *x*- and *y*-components of dipoles are much smaller. Note, however, that the average magnitude of the *y*-component of dipoles is larger than that of the *x*-component (such a relationship between them is very noticeable in Fig. 1 while the external field is relatively weak) – because the domains are *closure domains*, with the dipolar flux closing along the direction of the domains' alternation, i.e., along the *y* axis. Predicted in FE ultrathin films by direct first-principles calculations,[36] this local dipoles arrangement into flux-closure structures was recently experimentally established in PZT films.[37] Such an ideal domain system is illustrated in Fig. 2(a). Its stability is secured by the strong depolarizing field, and only a prevailing external field is able to distort the dipoles' configuration. The analysis given below traces the influence of the emerging applied field on dipoles' behavior.

4

1. *Stripe domains phase*

In the SD phase, the multidomain structure is almost intact [see image in Fig. 2(b)]. One can easily see from the diagram in Fig. 1 that, for fields up to 10^8 *V/m*, the *x*- and *y*-components of the dipole moments increase with different rate (*x*-components progress faster) while the *z*-components slightly decrease – with the total magnitude of the dipole moments remaining almost unchanged. The latter feature helps understand the character of the field influence inside this phase: a *rotation* of the individual dipoles away from the out-of-plane direction is induced with no substantial increase in the polar distortion. The diagram in Fig. 3(a) shows the extent to which the orientation of dipoles is affected: the averaged dipoles' direction (evaluated for the sites in the interior layers 5 to 8 to avoid the surface influence) with respect to the *x-y* plane is changing from *83.1ᵒ* to *67.8ᵒ* as the electric field gradually increases within the SD phase. Note that this angle with respect to the *x-y* plane is thereafter referred as to ϕ. Figure 3(b) reports the number of local dipoles having positive or negative *x*-, *y*-, and *z*-Cartesian components as a function of the field's magnitude. Such a diagram assists in getting a more comprehensive understanding of how the electric field influences the dipolar rotation, that is, causes a decline in the number of negative *x*- and *y*-components of the local dipole moments.

Remarkably, a 50% balance between the positive and negative *z*-components is preserved by the system within the SD phase – an imperative criterion[38,13,14] of a multidomain 'up' and 'down' environment having a vanishing out-of-plane macroscopic polarization [Fig. 4(a)]. Such a constancy of a multidomain structure illuminates the fact that depolarizing field (responsible for the domains existence) is still more superior to the external field. That is why we do not see any alteration in the average dipoles' *z*-component value (which is controlled by the depolarizing field) and no change in the average *y*-component value (which is responsible for the morphology of closure domains) until the field of 10^7 *V/m* is reached (see Fig. 1). Only with the applied field progressing beyond the 10^7 *V/m*, not vital deviations in the dipoles' components take place, more visible initially for the *x*-components. Indeed, images of dipoles' configuration in the field of 10^7 *V/m* (panel *b*) and in the field of 10^8*V/m* (panel *c*) presented in Fig. 2 confirm that in the field range up to 10^8 *V/m* the system has a strongly expressed multidomain structure. However, it also becomes apparent that an advancing electric field is producing a certain distortion in the dipoles arrangement. In particular, a formation of cylindrical bubbles[19] is underway (panel *c*) in the vicinity of domain walls – which is a region where the dipole moments are weaker in magnitude.[19]

Although the system in the SD phase does not possess any *out-of-plane* polarization, the *overall* polarization is not equal to zero [see Fig. 4(b)] thanks to the in-plane dipoles' components. In particular, the *x*-component of the polarization significantly increases with the applied electric field, which leads to an overall polarization being nearly oriented along the [100] direction (i.e., perpendicular to both the normal of the film and the domain wall propagation direction) as the *y*-component of polarization is close to zero.

2. *Dipolar waves phase*

Further increase in magnitude of the applied field leads to a series of truly amazing changes inside the system. Even though the dipoles' motion is still constrained by the depolarizing field, the growing external field takes progressively more control of their direction and magnitude. Such latter control brings destruction to the domain walls and leads to formation of *dipolar waves* (note that such waves have also previously been predicted to exist as a transitional step in *misfit-strain-induced* domain evolution[19]). Indeed, the escalating external field, having the in-plane components, is causing the growing dipoles' deflection toward the (*x-y*) plane. Essentially, the progression of the *y*-components' magnitude is the key condition for the *cylindrical* bubbles formation (in the domain wall region) around which the *dipolar waves* are shaped,[19] preventing a direct *stripe-to-bubble* phase transition typical for [001] electric field.[29]

As follows from Fig. 1, for fields larger than 10^8 *V/m,* all three dipole moment components are changing very fast in both their magnitudes and directions. This results in: (1) matching in their average *x*- and *y*-components magnitude in the field of $\sim 5 \times 10^8$ *V/m* (point K in Fig. 1), (2) disappearance of negative *x*- and then negative *y*-components [Fig. 3(b), fields 2×10^8 *V/m* and 4×10^8 *V/m*, respectively], and (3) termination of the 50% balance between the positive and negative *z*-components of the dipoles – the number of sites with positive *z*-components now surpasses the number of sites with negative ones [Fig. 3(b)] and it continues its surge thereafter.

Undoubtedly, the last factor, combined with the parity between the magnitudes of dipoles' *x*- and *y*-components can be seen as a signal of waning of a closed-flux multidomain structure (as it was mentioned above, there is no symmetry between the *x*- and *y*-directions in a "healthy" closed-flux multidomain environment, meaning that one of the dipoles' in-plane component – along the flux-closure direction – is always larger than the other, specifying the trend in which the domains propagate).

The *dipolar waves* become the next step in the structural evolution of the system. They are exposing a significant dipoles' rotation toward the *x-y* plane, explicitly confirmed by the diagram in Fig. 3(a) – angle is falling from 67.8^o for a field of 10^8 *V/m* to 22.5^o in the field of 5×10^8 *V/m*, followed by a rapid decline in their *z*-component values as indicated by Fig. 1. Thus, in the field range between 10^8 *V/m* and 5×10^8 *V/m,* dipoles are radically reoriented.

This pattern in the collective behavior of electric dipoles is noticeably displayed in Figs. 2: panel *c*, for the field of 10^8 *V/m*, shows the beginning of the DW phase which starts with the formation of cylindrical bubbles, the necessary condition for the dipolar waves existence;[19] panel *d*, for the field of 2×10^8 *V/m*, illustrates the state of the system when cylindrical bubbles reached the surface; panels *e-f*, for the field of 5×10^8 *V/m*, – further increase of the electric field results in gradual disappearance of cylindrical bubbles, the remnants of domain walls, and following penetration of positive region of the system into negative, indicating the beginning of BP (concurs with the matching of average magnitudes of dipoles *x-, y*-components, point K in Fig. 1).

The dipoles reorientation toward the *x-y* plane in growing electric field leads to the further development of the *in-plane* macroscopic polarization, rotating from close to

the [100] direction in the SD phase to the [110] direction in the DW region, as specified by Fig. 4(b), which is the direction of the in-plane component of the applied field itself. Thus, the magnitude distinction between two components of the in-plane polarization disappears at the end of the DW phase [Fig. 4(b)] as the projection along [110] direction becomes the only one permitted to the in-plane components of dipoles by the external field (Fig. 1).

Another important tendency in the system development should be mentioned for the DW state: the total average magnitude of dipole moments now *rises* with the field's strength upsurge – a sign of an amplified polar distortion prompted by the external electric field and unstoppable from now on (see Fig. 1). Definitely, the DW phase is a *turning point* in the domains transformation.

Interestingly, Figure 3(a) also shows that the orientation of dipoles with respect to the *x-y* plane can get below 45°, which may appear to be surprising at first when recalling that the external field that triggers their rotation is along the [111] direction. The understanding of this fact becomes straightforward once realizing that the evolution of a multidomain structure takes place in the setting of *two* interacting electric fields – the *depolarizing field* produced by the bound charges accumulated on the film surfaces and the *applied external field*. Obviously, their mutual orientation depends on the domain morphology. The net electric field, as a superposition of these two fields, is the background and the creating power that transforms the internal structure of the system.

3. Bubbles phase

As the rotation of dipoles advances, more and more of them are leaving the negative *z*-component region of the supercell (former down-domain), which inevitably leads to a misbalance between the positive and negative polarization charges accumulated on a given surface. Therefore, the symmetry in the distribution of depolarizing field in the system will be lost – a *net* depolarizing field in the negative *z*-direction will exist in the sample.

Apparently, it happens as soon as the equilibrium between the number of dipoles with negative *z*-components and the number of dipoles with positive *z*-components is broken. As follows from the diagram in Fig. 3(b), this event takes place in the external field between 2×10^8 *V/m* and 3×10^8 *V/m* and corresponds to the average dipoles' orientation with respect to *x-y* plane of $\sim 45^o$, as suggested by the diagram in Fig. 3(a).

This trend should convey two outcomes: (1) the total depolarizing field in the positive (negative) direction will increase (decrease) producing the net field rotation toward the *x-y* plane in both regions, which in its turn triggers the dipoles rotation toward the in-plane direction; (2) the region in the supercell occupied by the dipoles with negative *z*-components will shrink. This predicted development in the structural evolution of the system was entirely confirmed by the computational data.

Indeed, the diagram in Fig. 3(b) reveals fast reorientation of dipoles beyond the DW phase in progressing external field: the amount of dipoles with positive projection of their *z*-component is growing at a very quick rate. Such an expansion leads to

7

modification in the depolarizing field (and the net field) as described above and translates into (i) a reduction of the average magnitude of the *z*-component of the dipoles while increasing the magnitudes of the in-plane components (Fig. 1), (ii) further weakening of the depolarizing field in the down-domain region as a result of accelerated dipoles' rotation away from the out-of-plane direction [Fig. 3(a)] combined with decline in the number of dipoles with negative *z*-components [Fig. 3(b)], (iii) an elimination of the previously existing boundaries between the zones of dipoles with positive and negative *z*-components via an expansion of the region with positive dipoles (former up-domain) into the former down-domain neighborhood [as shown in Figs. 2(e) – front plane image, and 2(f) – 3-d image of the system, field 5×10^8 *V/m*], followed by division and further constriction of the areas filled with negative *z*-component dipoles – because of the gradual disappearance of the latter ones [Fig. 2(g) – 3-d image, field of 6×10^8 *V/m*]. All of these factors make the existence of dipolar waves impossible, but secure the system conversion into a new state – the *bubbles* phase.

In this state, as the field varies from 5×10^8 *V/m* to *1.4* $\times 10^9$ *V/m*, the bubbles, steadily shrinking areas of adjacent sites with negative *z*-dipoles, are the evidence of depolarizing field transformation, which makes it less dependent on the misfit strain and more and more the product of the mounting external field. Being *3-d clusters* of dipoles, having *z*-component orientation opposite to that of the external field, parted from each other into isolated islands, the bubbles are in fact the remnants of a multidomain structure – one more step down in the evolution from the multidomain state.

In the BP state, the (nearly) balance between the average magnitudes of the dipoles' negative and positive *z*-components disappears. A significant numerical growth of dipoles in the positive *z*-component region of the supercell (at the cost of the dipoles in the negative region) is transformed into gradual increase in their average magnitude. Subsequently, the total *out-of-plane* polarization is evolving [Fig. 4(a)], and this tendency becomes a permanent attribute of the system in the following development as the external field rise continues.

4. Transitional phase

With disappearance of the last signs of the down-domains – the bubbles, the system is shifting into a *transitional phase* (TP). It happens in the field of *1.4×10^9 V/m* when the dipoles' average *z*-components' value is at its lowest level (Fig. 1, point L), implicating that the average orientation of the dipoles is the closest to the in-plane [110] direction [that is, along the direction of the net field; see Fig. 3(a), angle $\phi = 5.5^o$].

The depolarizing field in the system has only one direction now – opposite to the *z*-component direction of the external field. Further increase in the external field will rotate the net field away from the *x-y* plane approaching it to the orientation of the applied field. It is understandable, that as long as the depolarizing field exists, the net field will never coincide with the external [111]-field.

The field of *1.4×10⁹ V/m* can be considered as a *critical field* in which the evolution of the system from the initial multidomain state is accomplished by completely eliminating the original collective behavior of dipoles. The last reminders of domains, the bubbles, are destroyed and remaining lone dipoles with negative *z*-components are now dispersed throughout the supercell [see Fig. 2(h)]. In this specific *transitional phase* of the system, although the multidomain structure is already destroyed, the *monodomain* state is not geared up yet – the net electric field is not homogeneous so far because of those few dipoles with negative *z*-components still existing throughout the system [Fig. 3(b)].

In the TP, the averaged magnitude of the *z*-components of the dipole moments is finally moving up (very visible in the initial part of the TP section of the phase diagram in Fig. 1) following the field escalation, the first time since the external field was introduced to the system. This increase is partially caused by the dipoles rotation away from the *x-y* plane, improving the average angle they form with [110] direction up to *5.8ᵒ* at the end of TP [Fig. 3(a)]. It becomes an extremely slow development while the very last 'negative' dipoles are converted into 'positive' (easy to observe in the second part of TP segment of the phase diagram in Fig. 1 – the plotted line for the average magnitude of the *z*-components of dipoles becomes almost flat).

5. *Monodomain phase*

The *monodomain* (MD) phase manifests itself with unstoppable increase of all the dipoles components' magnitudes (Fig. 1). The direction of dipole moments (now being the same for all the sites in the supercell, except those that are close to the surface in addition to having smaller magnitudes) tilts more and more away from the *x-y* plane toward the direction of the external applied field [see Fig. 3(a)]. Obviously, their orientation in the supercell is defined by the net field, meaning that they will never align along the direction of the applied field [see Fig. 3(a) that shows that the angle formed by the dipoles with respect to the *x-y* plane is only *10.5ᵒ* for an applied field of *5×10⁹ V/m*]. Indeed, Fig. 5(a), illustrating the atomistic picture of the dipoles configuration in this state, explicitly confirms that dipoles alignment is far-off the [111] direction of the external field. It becomes apparent that the interaction between the depolarizing field and the external field in the frame of the MD phase presents an opportunity to *control* both the direction of *polarization* and its magnitude by manipulating *only* the scale of the *applied field*.

To assess the action of depolarizing field in the MD phase, a simulation for the same system under *short-circuit-like* electrical boundary conditions (98% screening of depolarizing field) was performed (for an applied field of *5×10⁹ V/m*). In such conditions, when no polarization charges can accrue on the film surfaces, the dipoles are all aligned along the [111] direction – the direction of the applied field [Fig. 5(b), dipoles on the surfaces differ in their direction and are larger in magnitude as we should expect in the absence of polarization charges]. Besides, as one can see in Fig. 5(b), dipoles being freed of the suppressive action of depolarizing field (that has a direction opposite to the *z*-component of the dipole moments) become significantly larger in their magnitude. More precisely, it increases by *1.25* times as soon as the depolarizing field is removed according to computational data. Hence, by *varying* the *screening parameter* we can also *modulate* the *polarization* of a nanoferroelectric

sample in both the direction and magnitude in a rather significant range while keeping the applied field unchanged.

Overall, the *total* polarization averaged along the supercell evolves in accord with the external-field-induced evolution of dipoles' configuration – from close to zero initial value in the SD phase to *0.18 C/m^2* in the MD phase, for a field of *10^{10} V/m*, while rotating away from the in-plane direction [see Fig. 3(a) and Fig. 4(b)].

One can wonder if the ferroelectric order in a PZT film will survive such a powerful external field. Note that the real critical fields are expected to be smaller than those predicted here (Laudauer's paradox), because substrate-grown films are likely to exhibit defects that reduce such fields.[40,41] In addition, the *net* field inside the ferroelectric sample should be considered – the result of superposition of applied and depolarizing fields, which lessens the strength of the field that is actually affecting the ferroelectric structure.

B. AFD motion evolution

While discussing the behavior of electric dipoles under the influence of an external field, we did not focus on the AFD motion that each site of the supercell possesses. Nevertheless, the well-known *coupling* that exists between the *AFD tilting* and *polar distortion*[28] mutually rearranges the magnitude and direction of both of them to some extent, and certainly was affecting the dipoles conduct (and, therefore, the polarization) already examined above.

The diagram in Fig. 6(a) illustrates the evolution that the AFD motion undergoes when affected by the external field. Note that the AFD distortions in the studied system have both the in-plane and out-of-plane components as should be expected since the AFD vectors' orientation is known to follow to a certain degree the dipole's realignment[39] induced by the external field. Thus, they are neither pure "tilting" nor pure "rotation" of the oxygen octahedra,[42,43] and rather constitute an intermediate case between these two possibilities specific for the PZT sample used in this study.

One can easily observe some similarity between the AFD progression in Fig. 6(a) and the dipoles development in Fig. 1 within a certain field range. Indeed, the diagram in Fig. 6(a) presents an increase in magnitudes of the in-plane AFD components until the TP state is reached, to be exact, up to the field of *1.4×10^9 V/m*, which happens simultaneously with the enhancement of the magnitude of the dipoles' in-plane components. But similarity in the dipoles and AFD vectors behavior ends here, since the *z*-components of AFD vectors decline unstoppably during the entire range of the applied electric field.

The synchronized improvement in the values of *x*- and *y*-components of both the dipole moments and AFD vectors seems like a contradiction to the well-known competing behavior between these two constituents of the system. Nevertheless, there is a simple explanation to this phenomenon. An external field does not directly influence the AFD vectors, but manages them indirectly by affecting the dipoles in two ways: inducing their rotation and prompting the polar distortion. The advance in

10

dipole moments' value leads to the overall decrease in the magnitude of AFD tilting – the consequence of coupling between polar and non-polar degrees of freedom, while the dipoles' rotation away from the initial out-of-plane direction will affect the direction of AFD vectors,[39] meaning that the AFD motions will deflect toward the in-plane direction. This causes the decrease of their *z*-components' magnitude but an increase of their *x*- and *y*-components.

Note that the correlation between the dipoles' and AFD vectors' total magnitudes is a reproduction of their mutual competing behavior: as seen in Fig. 6(b), a continuous *increase* in the dipoles' magnitude is complemented by a steady *decrease* in the magnitude of AFD vectors – because insignificant increase of the in-plane components of AFD vectors cannot compensate more substantial decrease in their *z*-components (in the field range up to *1.4×10^9 V/m*), and therefore the total magnitude of AFD vectors is constantly falling.

Obviously, such a close-coupling relationship accompanied by a competing conduct between these two degrees of freedom, has an impact on dipoles' configuration already influenced by the external field, subduing the polarization and shifting the phase transitions to lower values of the applied field than it would be in the absence of oxygen octahedral rotation.

Once the electric-field-induced dipoles' rotation toward the in-plane is complete [angle 5.5^o on the diagram in Fig. 3(a), which corresponds to the point L in Fig. 1], all the AFD vectors' components decrease in magnitude with increase in the applied field [see after point N in Fig. 6(a)]. Such a relationship significantly restrains the AFD motion as the field progresses, and in the field of *10^{10} V/m* its overall magnitude is only around *1.5^o* (*0.026 rad*). Such small non-polar atomic distortions permit in the case of a huge electric field to disregard the AFD motion altogether and assume that the system retains one order parameter only – the polarization.

IV.   SUMMARY AND CONCLUSIONS

A strong electric field applied along the [111] direction to a system of nanostripe ferroelectric domains is able to influence the dipoles' collective behavior by affecting their magnitude and direction. Consequently, the induced rearrangement in dipoles' configuration is leading to phase transitions; in total, 5 states were revealed through which the system evolves as the external field progresses. These phases are representing variations of dipoles collective behavior in a ferroelectric ultrathin film under the OC electrical boundary conditions. Therefore, our investigation allows predicting the properties of electric-field-influenced multidomain structures, which may become important in the view of reliability of nanoferroelectric-based electronic devices operating in the environment of strong electric fields. Such fields should be avoided if the multidomain configuration needs to be preserved, or can be used to intentionally modify the structure of the film and, thus, manipulate macroscopic property such as polarization – in both the magnitude and direction. When coupled with adjusting the screening parameter (to amend the residual depolarizing field), the range of regulating the polarization will be even broader. Thus, the results of this investigation, in addition to widening our knowledge about fundamental properties of

ultrathin ferroelectric films, may have wide-ranging implications for the application and development of high-performance electronic devices.

---

[1] J. F. Scott, Annu. Rev. Matter. Sci. **28**, 79 (1998).

[2] D. Fong, G. Stephenson, S. Streiffer, J. Eastman, O. Auciello, P. Fuoss, and C. Thompson, Science **304**, 1650 (2004).

[3] J. Junquera and P. Ghosez, Nature (London) **422**, 506 (2004).

[4] M. Dawber, K. M. Rabe, and J. F. Scott, Rev. Mod. Phys. **77**, 1083 (2005).

[5] I. Kornev, H. Fu, and L. Bellaiche, J. Mater. Sci. **41**, 137 (2006).

[6] K. Rabe, Ch. H. Ahn, and J.-M. Triscone, *Physics of Ferroelectrics:A Modern Perspective*, volume 105 of topics in Applied Physics, (Springer, Berlin, 2007).

[7] N. Setter *et al.*, J. Appl. Phys. **100**, 051606 (2006).

[8] K. Kim and Y. J. Song, Microelectron. Reliab. **43**, 385 (2003).

[9] D. Dimos and C. H. Mueller, Annu. Rev. Mater. Sci. **28**. 397 (1998).

[10] J. F. Scott, *Ferroelectric Memories* (Springer, Berlin, 2000).

[11] J. F. Scott, Science **246**, 1400 (1989).

[12] S. Prosandeev, I. Ponomareva, I. Naumov, I. Kornev, and L. Bellaiche, J. Phys.: Condens. Matter **20**, 193201 (2008).

[13] I. Kornev, H, Fu, and L. Bellaiche, Phys. Rev. Lett. **93**, 196104 (2004).

[14] S. K. Streiffer, J. A. Eastman, D. D. Fong, Carol Thompson, A. Munkholm, M. V. Ramana Murty, O. Auciello, G. R. Bai, and G. B. Stephenson, Phys. Rev. Lett. **89**, 067601 (2002).

[15] G. Catalan *et al.*, Rev. Mod. Phys. **84**, 119 (2012).

[16] K. Uchino, *Piezoelectric actuators and Ultrasonic Motors* (Kluver Academic, Boston, 1996).

[17] B. Noheda, D. E. Cox, G. Shirane, S.-E. Park, L. E. Cross, and Z. Zhong, Phy. Rev. Lett. **86**, 3891 (2001).

[18] L. Bellaiche, A. Garcia, and D. Vanderbilt, Phys. Rev. Lett. **84**, 5427 (2000); Ferroelectrics **266,** 41 (2002).

[19] D. Sichuga and L. Bellaiche, Phys. Rev. Lett. **106**, 196102 (2011).

[20] D. G. Schlom *et al.*, Annu. Rev. Mater. Res. **37**, 589 (2007).

[21] I. Kornev, L. Bellaiche, P.-E. Janolin, B Dkhil, and E. Suard, Phys. Rev. Lett. **97**, 157601 (2006).

[22] M. Fornari and D. J. Singh, Phys. Rev. B **63**, 092101 (2001).

[23] B. Noheda, L. Wu, and Y. Zhu, Phys. Rev. B **66**, 060103(R) (2002).

[24] D. M. Hatch, H. T. Stokes, Rajeev Ranjan, Ragini, S. K. Mishra, Dhananjai Pandey, and Brendan J. Kennedy, Phys. Rev. B **65**, 212101 (2002).

[25] D. I. Woodward, J. Knudsen, and I. M. Reaney, Phys. Rev. B **72**, 104110 (2005).

[26] Rajeev Ranjan, S. K. Mishra, Dhananjai Pandey, and Brendan J. Kennedy, Phys. Rev. B **65**, 060102(R) (2002).

[27] J. M. Rondinelly and Nicola Spaldin, Adv. Mater. **23**, 3363 (2011).

[28] D. Vanderbilt, and Z. Zhong, Ferroelectrics **206**, 181 (1998).

[29] Bo-Kuai Lai, I. Ponomareva, I. I. Naumov, I. Kornev, Huaxiang Fu, L. Bellaiche, and G. J. Salamo, Phys. Rev. Lett. **96**, 137602 (2006); Bo-Kuai Lai, Inna Ponomareva, Igor A. Kornev, L. Bellaiche, and G. J. Salamo, Phys. Rev. B **75**, 085412 (2007).

[30] M. Kisilewski, A. Maziewski, T. Polyakova, and V. Zabotskii, Phys. Rev. B **69**, 184419(2004).

[31] F. Iikawa, M. Knobel, P. V. Santos, C. Adriano, O. D. D. Couto, M. J. S. P. Brasil, C. Giles, R. Magalhães-Paniago, and L. Däweritz, Phys. Rev. B **71**, 045319(2005).

[32] D. Sichuga, I. Ponomareva, and L. Bellaiche, Phys. Rev. B **80**, 134116 (2009).

[33] I. Ponomareva, I. I. Naumov, I. Kornev, Huaxiang Fu, and L. Bellaiche,Phys. Rev. B **72**, 140102(R) (2005).

[34] W. Zhong, D. Vanderbilt, K. M. Rabe, Phys. Rev. B **52**, 6301 (1995); W. Zhong, D. Vanderbilt, K. M. Rabe, Phys. Rev. Lett. **73**, 1861(1994).

[35] L. Bellaiche, A. Garcia, and D. Vanderbilt, Phys. Rev. B **64**, 060103(R) (2001).

[36] P. Aguado-Puente and J. Junquera, Phys. Rev. Lett. **100**, 177601 (2008).

[37] C.-L. Jia, K. W. Urban, M. Alexe, D. Hesse, and I. Vrejoiu, Science **331**, 1420 (2011).

[38] M. E. Lines, A. M. Glass, *Principles and Applications of Ferroelectrics and Related Materials* (Clarendon Press, Oxford, 1977).

[39] D. Sichuga, W. Ren, S. Prosandeev, and L. Bellaiche, Phys. Rev. Lett. **104**, 207603 (2010).

[40] R. Landauer, J. Appl. Phys. **28**, 227 (1957).

[41] S. Lisenkov, D. Rahmedov, and L. Bellaiche, Phys. Rev. Lett. **103**, 047204 (2009).

[42] A. M. Glazer, Acta Crystallogr. Sect. B **28**, 3384 (1972).

[43] A. M. Glazer, Acta Crystallogr. Sect. A **31**, 756 (1975).

FIGURE CAPTIONS

FIGURE 1 (Color online): Electric-field-induced evolution of the absolute value of the Cartesian conponents of the local dipole moments, and their magnitude, in the studied compressively-strained, 4.8 nm-thick (001) PZT film at 10 K. The vertical dashed lines delimit the different regions. A logarithmic scale is used for the electric field (abscissa) axis.

FIGURE 2 (Color online): Examples of microstructures in the investigated 4.8 nm-thick PZT film at 10 K. Panel *a* depicts the domains structure in the absence of external field. Panels *b-i* correspond to applied electric fields of 10^7 *V/m* (SD phase), 10^8 *V/m* (beginning of DW phase), 2.0×10^8 *V/m* (DW phase, cylindrical bubbles reach the surface), 5.0×10^8 *V/m* (beginning of BP, front plane image in panel *e* and 3-d image in panel *f*), 6.0×10^8 *V/m* (BP, 3-d image in panel *g*), 1.4×10^9 *V/m* (beginning of TP), respectively. The cylindrical bubbles are highlighted by means of ovals in panel *c*. Arrows down (red) and up (blue) represent the orientations of dipoles with positive and negative *z*-components, respectively. In panels *a-e*, multiple arrows at each site are the result of projections in (*z-y*) plane of all the dipoles that lie in the same line along *x* axis, having slightly different orientation at each site.

FIGURE 3 (Color online): 10 K properties related to the dipoles' rotation in the studied (001) PZT film as a function of magnitude of the external electric field applied along the [111] direction. Panel *a* shows the average angle made by the dipoles with the (001) plane. Panel *b* displays the number of dipoles with positive (respectively, negative) *x*-, *y*-, and *z*-components that are denoted here as X+, Y+, and Z+ (respectively, X-, Y-, and Z-), respectively. A logarithmic scale is used for the electric field (abscissa) axis.

FIGURE 4 (Color online): Electric-field-induced evolution of the out-of-plane components of the polarization in the investigated compressively-strained PZT film at 10 K. Panel *a* illustrates the total *z*-component of polarization as well as the separate contribution from the dipoles having positive or negative *z*-components. Panel *b* displays the same information that panel *a* but for the total polarization. A logarithmic scale is used for the electric field (abscissa) axis.

FIGURE 5 (Color online): Monodomain state seen in a (*z-y*) plane at 10 K, in the studied PZT thin film under an external electric field of 5×10^9 *V/m* magnitude and applied along [111]. Panels *a* and *b* correspond to open-circuit and short-circuit electrical boundary conditions, respectively.

FIGURE 6 (Color online): Evolution of the average absolute value of the local AFD vector components (panel *a*) and evolution of the averaged magnitude of these local AFD vectors (panel *b*) as a function of magnitude of the external electric field in the studied (001) PZT film at 10 K. Panel *b* also displays the corresponding evolution of

14

the average magnitude of the local dipole moments for comparison. A logarithmic scale is used for the electric field (abscissa) axis.
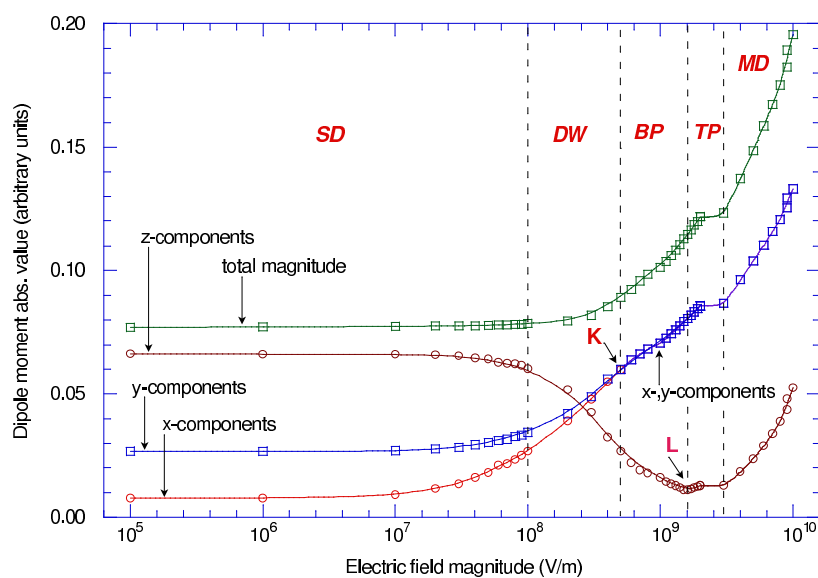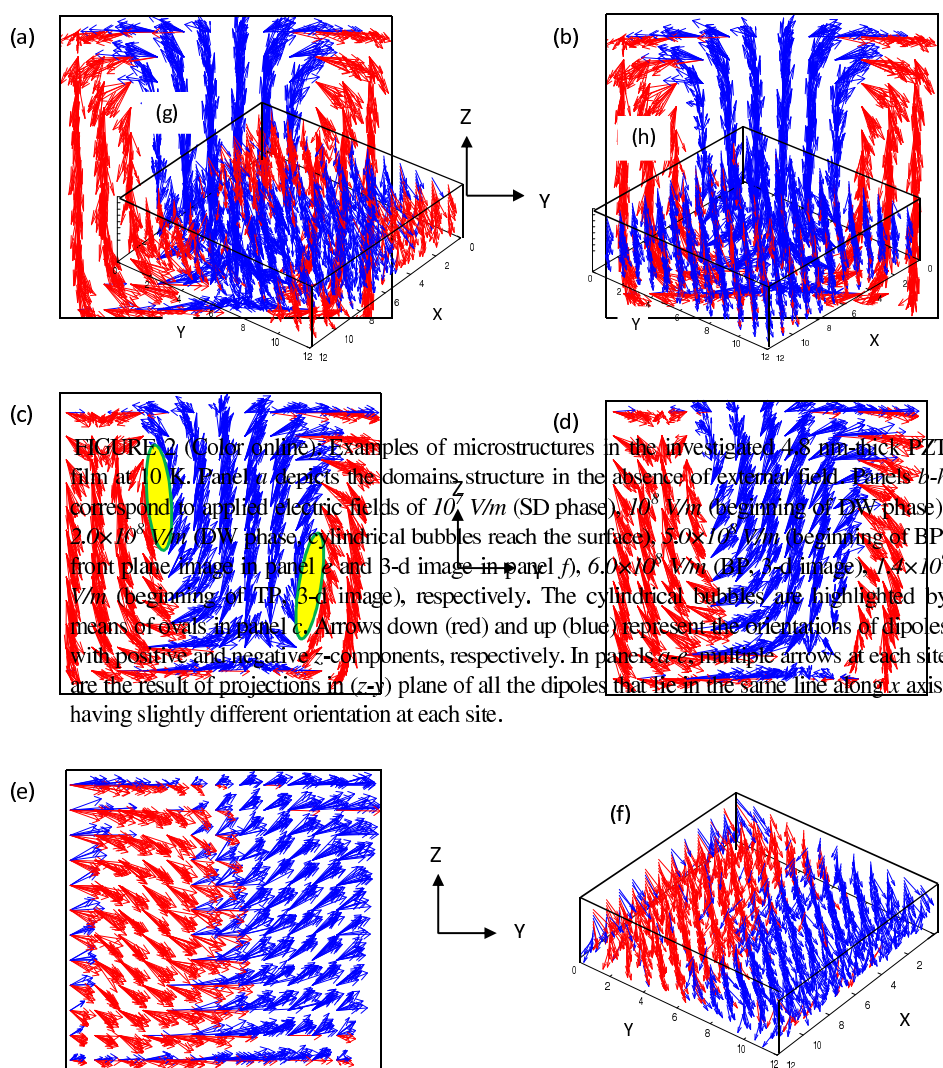
FIGURE 1 (Color online): Electric-field-induced evolution of the absolute value of the Cartesian conponents of the local dipole moments, and their magnitude, in the studied compressively-strained, 4.8 nm-thick (001) PZT film at 10 K. The vertical dashed lines delimit the different regions. A logarithmic scale is used for the electric field (abscissa) axis.

Figure 1   BQ11619   22MAY2012

FIGURE 2. (Color online) Examples of microstructures in the investigated 4.8 nm-thick PZT film at 10 K. Panel a depicts the domains structure in the absence of external field. Panels b-h correspond to applied electric fields of 10^7 V/m (SD phase), 10^8 V/m (beginning of DW phase), 2.6×10^8 V/m (DW phase, cylindrical bubbles reach the surface), 3.0×10^8 V/m (beginning of BP, front plane image in panel e and 3-d image in panel f), 6.0×10^8 V/m (BP, 3-d image), 1.4×10^9 V/m (beginning of TP, 3-d image), respectively. The cylindrical bubbles are highlighted by means of ovals in panel c. Arrows down (red) and up (blue) represent the orientations of dipoles with positive and negative z-components, respectively. In panels a-g, multiple arrows at each site are the result of projections in (z-y) plane of all the dipoles that lie in the same line along x axis, having slightly different orientation at each site.
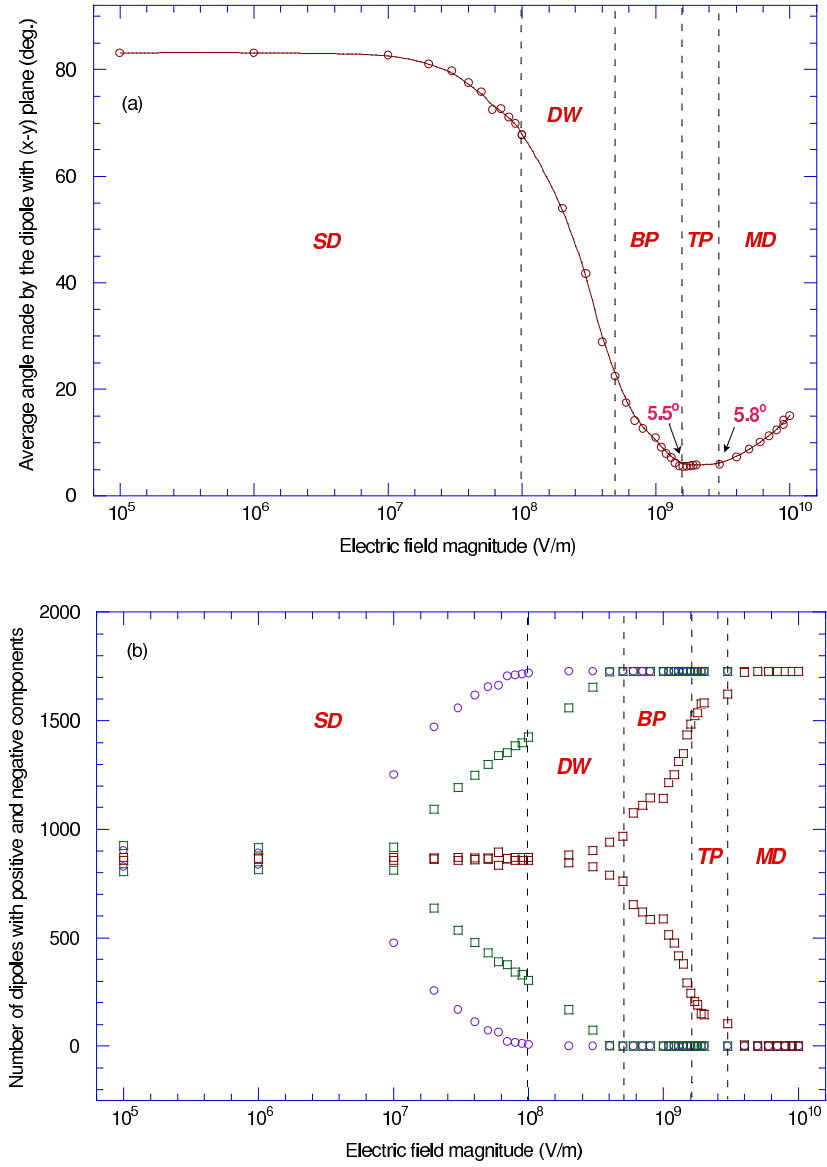
Figure 2   BQ11619   22MAY2012

FIGURE 3 (Color online): 10K properties related to the dipoles' rotation in the studied (001) PZT film as a function of the magnitude of the external electric field applied along the [111] direction. Panel *a* shows the average angle made by the dipoles with the (001) plane. Panel *b* displays the number of dipoles with positive (respectively, negative) x-, y- and z-components that are denoted here as X+, Y+ and Z+ (respectively, X-, Y- and Z-), respectively. A logarithmic scale is used for the electric field (abscissa) axis.
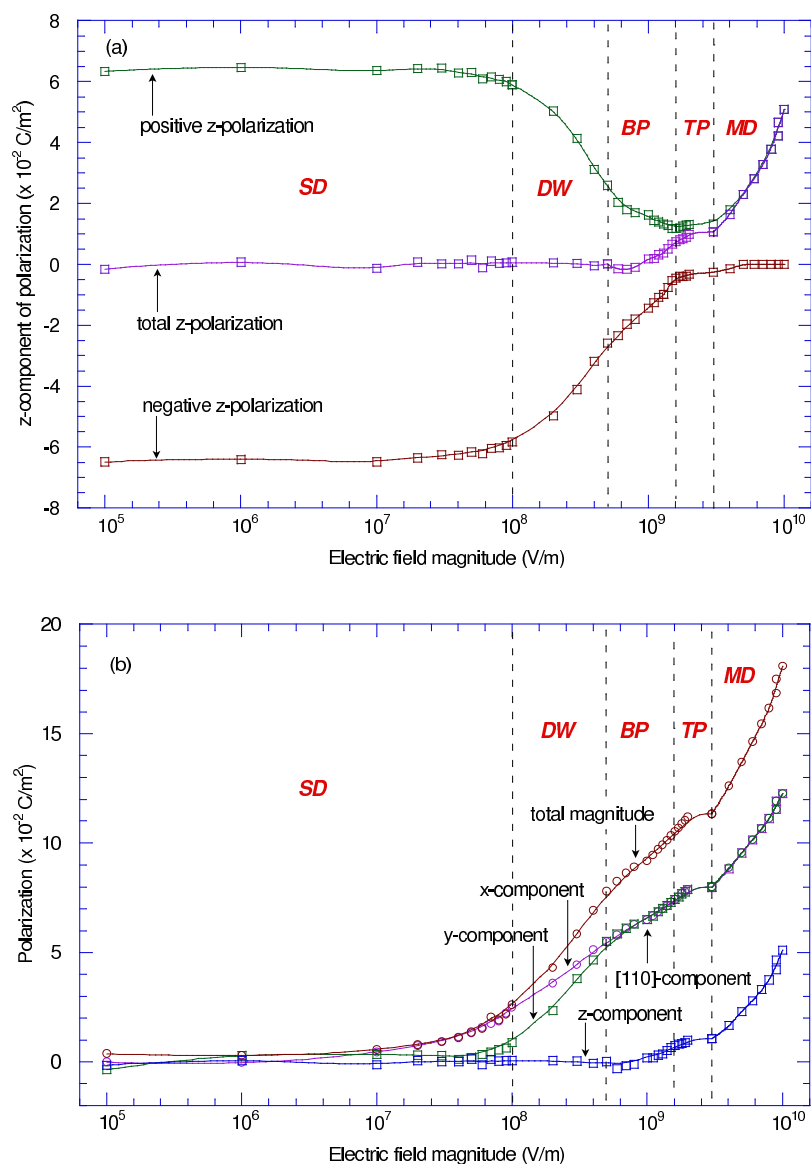
Figure 3   BQ11619   22MAY2012

FIGURE 4 (Color online): Electric-field-induced evolution of the out-of-plane components of the polarization in the investigated compressively-strained PZT film at 10K. Panel *a* illustrates the total *z*-component of polarization as well as the separate contribution from the dipoles having positive or negative *z*-components. Panel *b* displays the same information that panel *a* but for the total polarization. A logarithmic scale is used for the electric field (abscissa) axis.
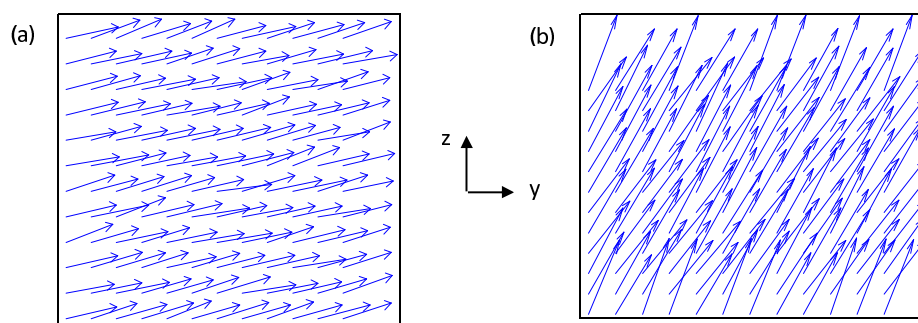
Figure 4   BQ11619   22MAY2012

FIGURE 5 (Color online): Monodomain state seen in a (z-y) plane at 10 K, in the studied PZT thin film under an external electric field of $5{\times}10^9$ V/m magnitude and applied along [111]. Panels *a* and *b* correspond to open-circuit and short-circuit electrical boundary conditions, respectively
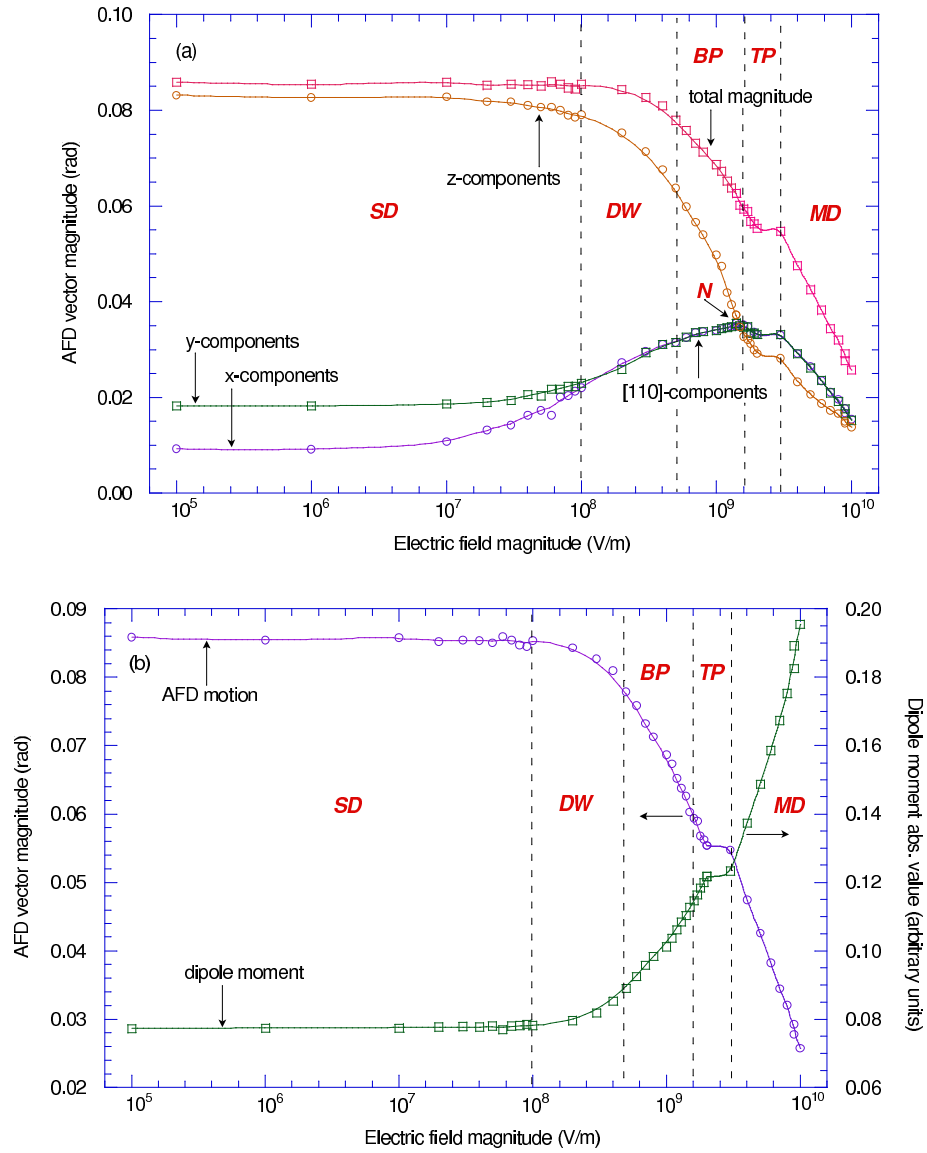
Figure 5   BQ11619   22MAY2012

FIGURE 6 (Color online): Evolution of the average absolute value of the local AFD vector components (panel *a*) and evolution of the averaged magnitude of these local AFD vectors (panel *b*) as a function of the magnitude of the external electric field in the studied (001) PZT film at 10 K. Panel *b* also displays the corresponding evolution of the average magnitude of the local dipole moments for comparison. A logarithmic scale is used for the electric field (abscissa) axis.

Figure 6   BQ11619   22MAY2012